COLLÈGE DE FRANCE
Laboratoire de Physique Corpusculaire

LPC 94 29

A LARGE AREA RICH FOR LONG BASELINE NEUTRINOS

D. Hatzifotiadou
CERN, Genève et World Laboratory, Lausanne

F. Block
CERN, Genève et INFN, Bologna

L. Cifarelli
CERN, Genève, et Universita di Pisa

J. Séguinot, T. Ypsilantis
Collège de France, Paris

A. Zichichi
CERN, Genève

COLLEGE DE FRANCE, IN2P3-CNRS, Laboratoire de Physique Corpusculaire,
11 Place Marcelin Berthelot, F-75231 Paris Cedex 05, FRANCE

CERN-LAA/PI-94-17
College de France LPC/94-29
24/6/94

A LARGE AREA RICH FOR LONG BASELINE NEUTRINOS

D. Hatzifotiadou[1,4], F. Block[1,2], L. Cifarelli[1,3], J. Seguinot[5], T. Ypsilantis[5] and A. Zichichi[1]

1) CERN, LAA Project, Geneva, Switzerland
2) INFN, Bologna, Italy
3) Physics Department, University of Pisa, Italy
4) World Laboratory, Lausanne, Switzerland
5) Collège de France, Paris, France

Abstract

A large RICH counter can serve as both target and detector for a long baseline neutrino oscillation experiment. A cylindrical radiator 20 m in diameter and 50 m long filled with Argon gas at (15 bar, 293K) has Cherenkov threshold γ_{th}=10 and contains 400 tons of sensitive target for neutrino interactions. A throughgoing β=1 particle will produce 4000 photoelectrons on a ring image and determine particle momentum to 4% at 20 GeV (assuming particle identification). The RICH image also determines the particle direction hence p_t as well as p, thus direct (from ν_μ) and indirect muons (from ν_τ) can be separated by cuts in the (p, p_t) plane.

A Monte Carlo simulation of RICH images has been made using a new algorithm inside GEANT to generate Cherenkov photons. A pattern recognition method based on a stereographic projection is presented. From the reconstructed Cherenkov angle the particle velocity is determined while, at the same time, particle identification is obtained from the width of the Cherenkov angle distribution. The width is mass dependant for particles of the same velocity because the Cherenkov angle error is dominated by multiple scattering, thus the RICH counter can determine particle type as well as momentum.

1. INTRODUCTION

One of the most important questions in neutrino physics is the problem of neutrino masses and mixing. The search for neutrino oscillations is thus a topic of increasing interest. These experiments use either atmospheric neutrinos or neutrino beams from accelerators with each type sensitive to a different range of values of neutrino masses (m_ν) and mixing angles (θ), thus exploring different areas of the (m_ν, θ) parameter space [1]. The apparatus described and studied here has been conceived as a potential experiment in the Gran Sasso underground Laboratory, at a distance of 731 km from CERN. The possibility for such an experiment was already among the physics goals of the Gran Sasso Project [2] and special care was taken to build the experimental halls aligned towards CERN. An advantage of a long baseline neutrino experiment is, of course, the increased sensitivity to small mass differences. Since the detector is directional and the beam is pulsed, the background should be negligible. Clearly, one must maximize the neutrino flux and target mass to obtain adequate statistics.

For such an experiment the large RICH counter, shown schematically in Fig. 1, can serve simultaneously as a target and detector. A cylindrical radiator, 20 m in diameter and 50 m in length filled with Argon gas at (15 bar, 293K) contains 400 tons of sensitive target for neutrino interactions. The mirror for reflecting the photons is spherical with a radius of $r_m=R_M=100$ m. The photon detector is taken to be on the focal surface of the mirror, namely on an upstream spherical surface $r=R_D=50.13$ m in radius [3]. The pixel size considered is 30x30 mm^2 thus, the detector has $3\cdot10^5$ channels (similar to proposed RICH detectors for B-Factories [4]). Downstream from the radiator and mirror we require a large surface area tracking device equipped with an iron absorber to identify muons and measure the direction of secondary charged particles and so determine the interaction vertex. A throughgoing $\beta=1$ charged particle in the radiator will produce 4000 points on the

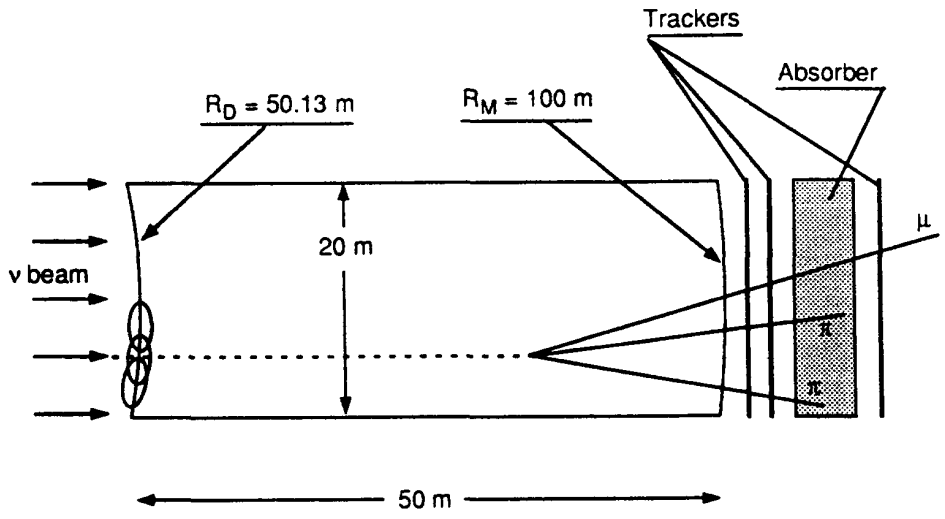

Fig. 1. A schematic view of the radiator, mirror and detector with the external tracker and absorber.

ring image with a radius of 4.8 m with good image quality even for an impact parameter x_e=10 m [3]. The Cherenkov angle chromatic error in Argon gas is 0.7 mrad whereas, for 30x30 mm^2 pixels, the pixel error is 0.17 mrad. Due to the unusually long radiator length (50 m) multiple scattering is not negligible and its contribution to the total angular error is dominant. As explained in Section 4, we use this fact to obtain particle identification.

2. THE SIGNATURE FOR NEUTRINO OSCILLATIONS

The combination of a RICH counter with an external tracker will determine the charged particle momentum and direction. We propose to identify direct muons ($\nu_\mu X \rightarrow \mu X'$) from indirect muons ($\nu_\tau X \rightarrow \tau X'$, $\tau \rightarrow \mu \nu_\tau$) on the basis of p and p_t measurements since their correlations are different. We have simulated the production of indirect muons from charged current (CC) ν_τ interactions with subsequent muonic decay of the tau ($\nu_\tau X \rightarrow \tau X'$, $\tau \rightarrow \mu \nu_\tau$) compared to direct muon production from CC ν_μ interactions ($\nu_\mu X \rightarrow \mu X'$) [5].

In the search for neutrino oscillations, $\nu_\mu \rightarrow \nu_\tau$, the former is the signal whereas the latter is the background.

For any initial neutrino energy, background muons tend to have higher p (for a given p_t) than do the signal muons thus, cuts in the (p, p_t) plane can discriminate between the two processes (see § 5). The CHORUS experiment will distinguish between these processes by measuring missing p_t with calorimetry [6].

3. STEREOGRAPHIC PROJECTION A OF CHERENKOV RING

A neutrino interaction produces few above threshold charged particles which then produce Cherenkov light on a conical surface. The axis of the cone is along the direction of the particle trajectory and the cone angle θ is given by $\cos\theta=1/n\beta$, where β is the particle velocity. After reflection on the spherical mirror, the image formed on the spherical detector surface is a circle [3]. Since it is not easy to display images on a spherical surface we use instead the stereographic projection because the projection of a circle on a spherical surface is also a circle on the stereographic plane.

The stereographic projection (see Fig. 2) has the stereographic plane tangent to the north pole N. A straight line from the south pole S of the detector sphere which passes through an image point P on the detector surface intersects the stereographic plane at point P'. The transformation which maps P (x, y, z) into P'(x_s, y_s, z_s) is

$$x_s = 2x/(1+z/r) \qquad (1)$$
$$y_s = 2y/(1+z/r)$$
$$z_s = r$$

where $r=\sqrt{(x^2+y^2+z^2)}$ is the radius of the detector sphere and O is the origin of the coordinate systems.

Since circles on a sphere can be described as the intersection of a cone with the spherical surface, a point (x, y, z) on the sphere can be expressed as a function of the cone angle α (the Cherenkov angle θ) and the azimuthal angle β (the Cherenkov angle ϕ).It can

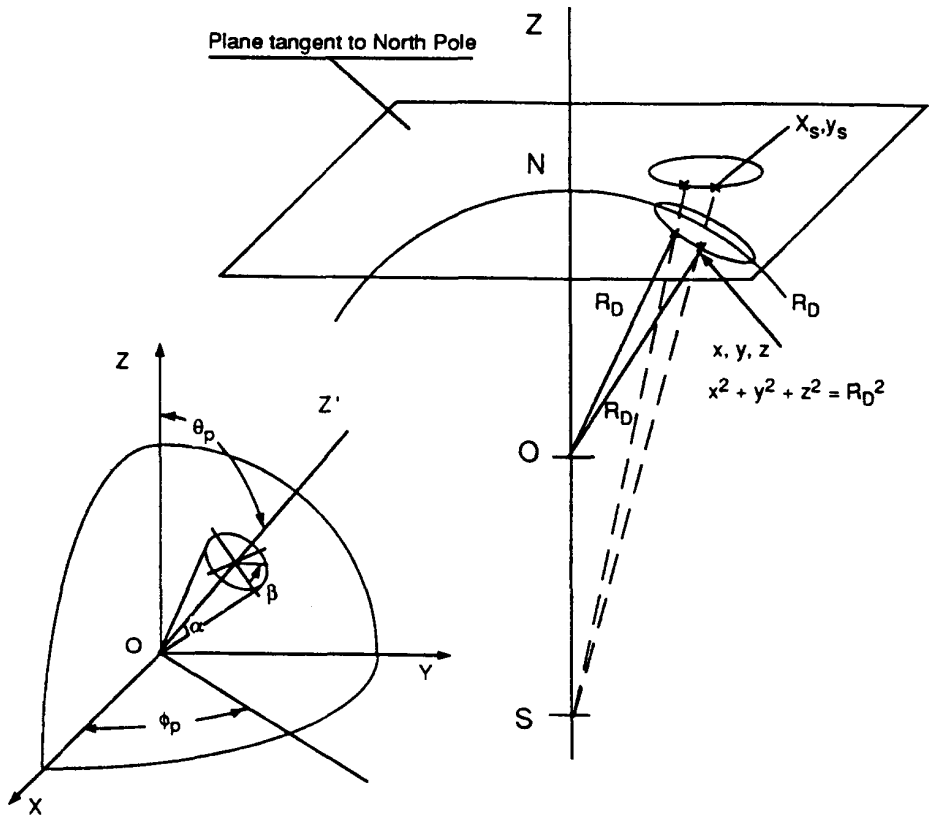

Fig. 2. A view of a stereographic projection. N and S are the north and south poles of the detector sphere of radius r. The inset shows a Cherenkov cone intersecting the detector sphere with cone angle (α) and circumferential angle (β).

be shown that the stereographic projection of a circle on sphere is a circle on the stereographic plane. The radius r_s and the center (x_o, y_o) of this circle are given by the following relations

$$(x_s-x_o)^2+(y_s-y_o)^2=r_s^2 \qquad (2)$$

$$x_o=\varepsilon r\cos\phi_p,\ y_o=\varepsilon r\sin\phi_p$$

$$r_s=2r\sin\alpha/(\cos\alpha+\cos\theta_p)$$

$$\varepsilon=2\sin\theta_p/(\cos\alpha+\cos\theta_p)$$

We show in Fig. 3, stereographic Cherenkov ring images of single CC events (3a, b, c are $\nu_\tau p$ events and 3d is a $\nu_\mu p$ event).

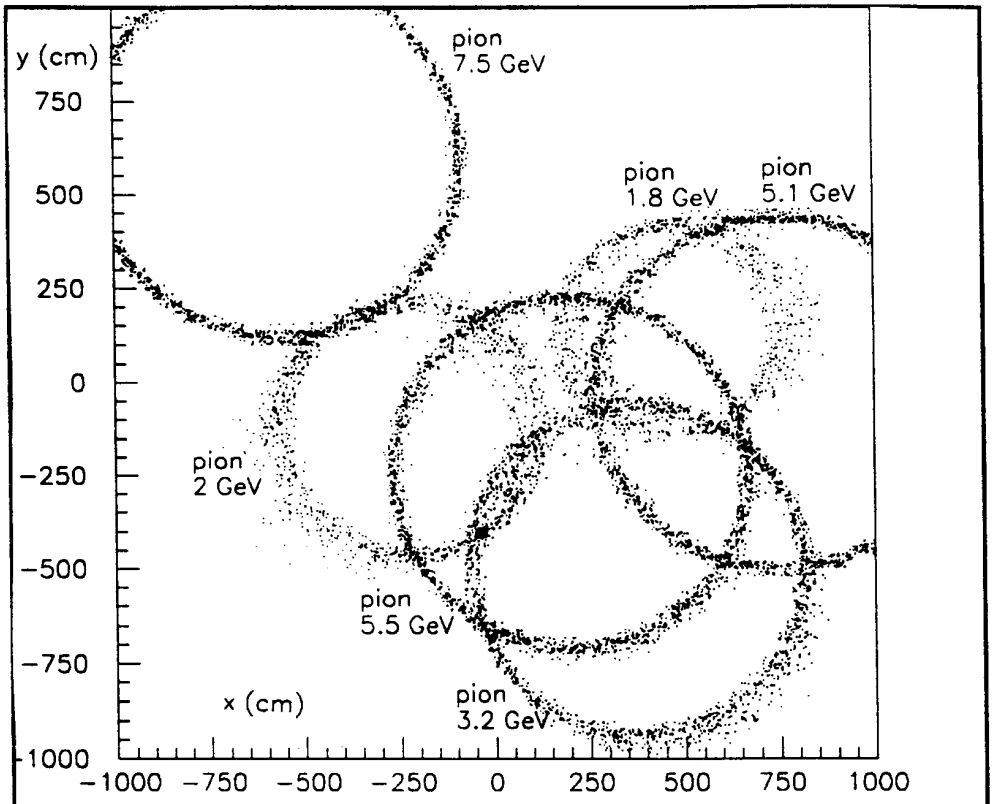

Fig. 3a. Stereographic Cherenkov images of an event $\nu_\tau X \to \tau^- \rho^0 \rho^0 \eta' \pi^+ p$, $\tau^- \to \nu_\tau \rho^- \to \nu_\tau \pi^- \pi^0$, $\rho^0 \to \pi^+ \pi^-$, $\eta' \to \pi^+ \pi^- \eta$, $\eta \to 3\pi^0$ (E_ν=40 GeV, z=25 m).

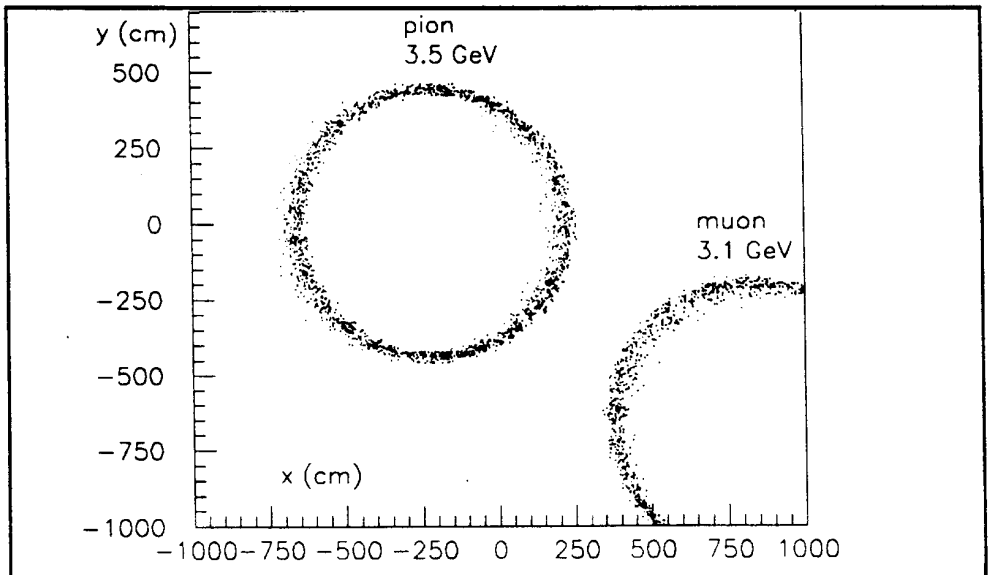

Fig. 3b. Stereographic Cherenkov images of an event $\nu_\tau p \to \tau^- \rho^0 \Delta^{++} \eta'$, $\tau^- \to \mu^- \nu_\tau \nu_\mu$, $\rho^0 \to \pi^+ \pi^-$, $\Delta^{++} \to p\pi^+$, $\eta' \to \pi^+ \pi^- \eta$, $\eta \to \gamma\pi^+\pi^-$ (E_ν=20 GeV, z=25 m).

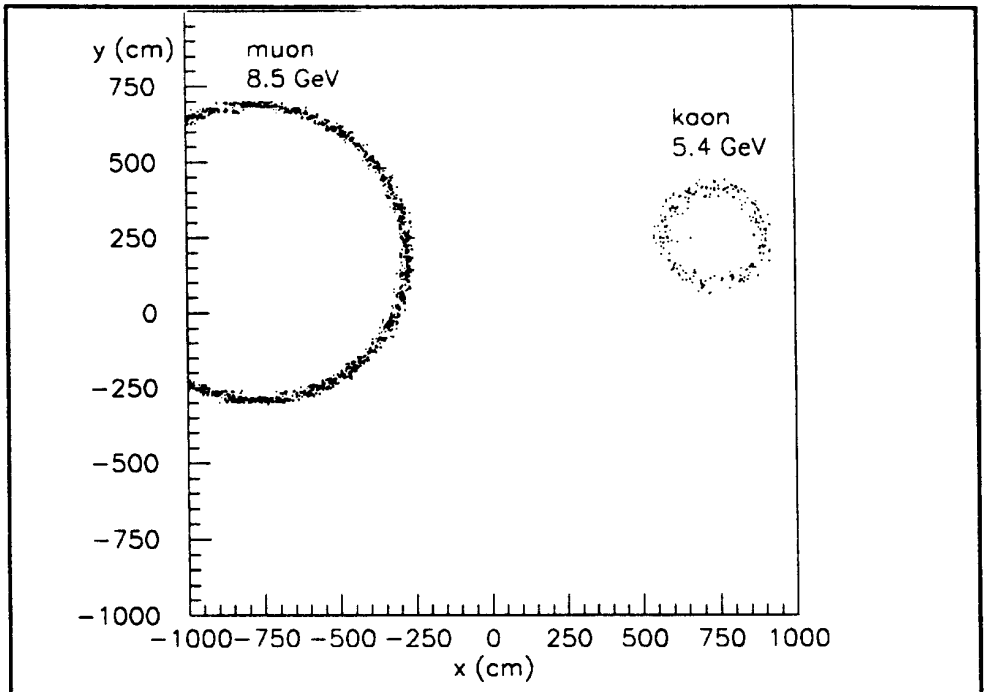

Fig. 3c. Stereographic Cherenkov images of an event $\nu_\tau p \rightarrow \tau^- K^+ K^- \Delta^{++} \eta$, $\tau^- \rightarrow \mu^- \nu_\tau \nu_\mu$, $\Delta^{++} \rightarrow p\pi^+$, $\eta \rightarrow \gamma\gamma$ (E_ν=20 GeV, z=25 m).

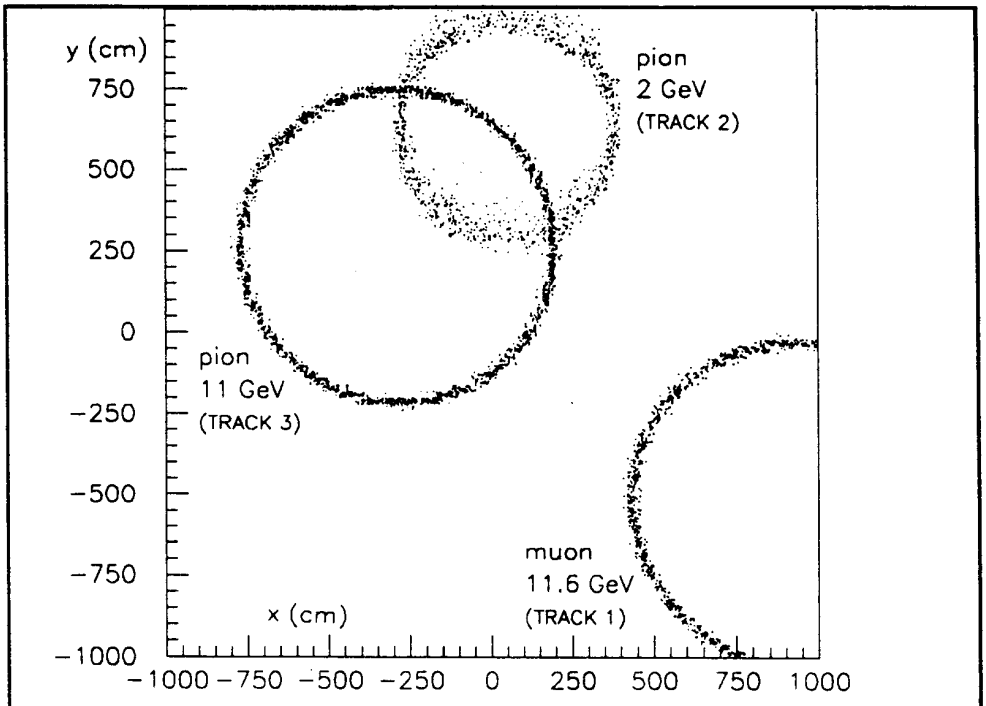

Fig. 3d. Stereographic Cherenkov images of an event $\nu_\mu p \rightarrow \mu^- \rho^+ \eta' \Delta^+ \pi^o$, $\rho^+ \rightarrow \pi^+ \pi^o$, $\Delta^+ \rightarrow \pi^+ \pi^o$, $\eta' \rightarrow \gamma\rho^o \rightarrow \gamma\pi^+\pi^-$ (E_ν=40 GeV, z=25 m).

3.1 PATTERN RECOGNITION & ANGLE RECONSTRUCTION

A Cherenkov ring is comprised of a number of hit points on the detector sphere with coordinates (x, y, z). We need to identify the rings and attribute each point to its proper ring. Due to the generally large number of points, pattern recognition based on a stereographic projection turns out to be relatively easy.

For each charged particle we calculate the center (x_o, y_o) of each stereographic circle from Eq. 2 using θ_p and ϕ_p as determined by the external tracker and assuming $\alpha=\theta_m=96$ mrad (the maximum Cherenkov angle for $\beta = 1$ particles at the average detected photon energy $<E>=6.7$ eV). By comparing the pattern of these centers (x_o, y_o) with the observed rings, one can easily tag those particles (below threshold) which have not produced rings.

We then combine each photon with each accepted charged particle and calculate r_s and the center point (x_o, y_o) from Eq.'s 2. The distribution of r_s values for a given track has a peak due to the real signal photons with a combinatorial continuum background (see Fig. 4.a, b). For each distribution of r_s we find the peak value $<r_s>$ and its rms width σ=FWHM/2.35 and then recalculate r_s using only those photons for which r_s is within $<r_s>\pm 3\sigma$. This identifies photons attributable to this track. Unambiguous photons are those that can be attributed to only one track. Pattern recognition thus consists of selection of unambiguous photons. In Fig. 4.c, d we show the r_s distribution of such photons.

At this point we have attributed a certain number of photons to each ring and can now reconstruct the Cherenkov angle θ based on the stereographic projection. Using only the accepted photons we make a least square fit and calculate the radius r_s and the center (x_0, y_0) and from r_s and $r_0^2=x_0^2+y_0^2$ we find the cone angle α

$$\tan\alpha = 4rr_s/(4r^2 - r_s^2 + r_0^2) \qquad (3)$$

The Cherenkov angle θ is taken as α but this is strictly true only for $x_c=0$. The particle polar and azimuthal angles (θ_p, ϕ_p) are then

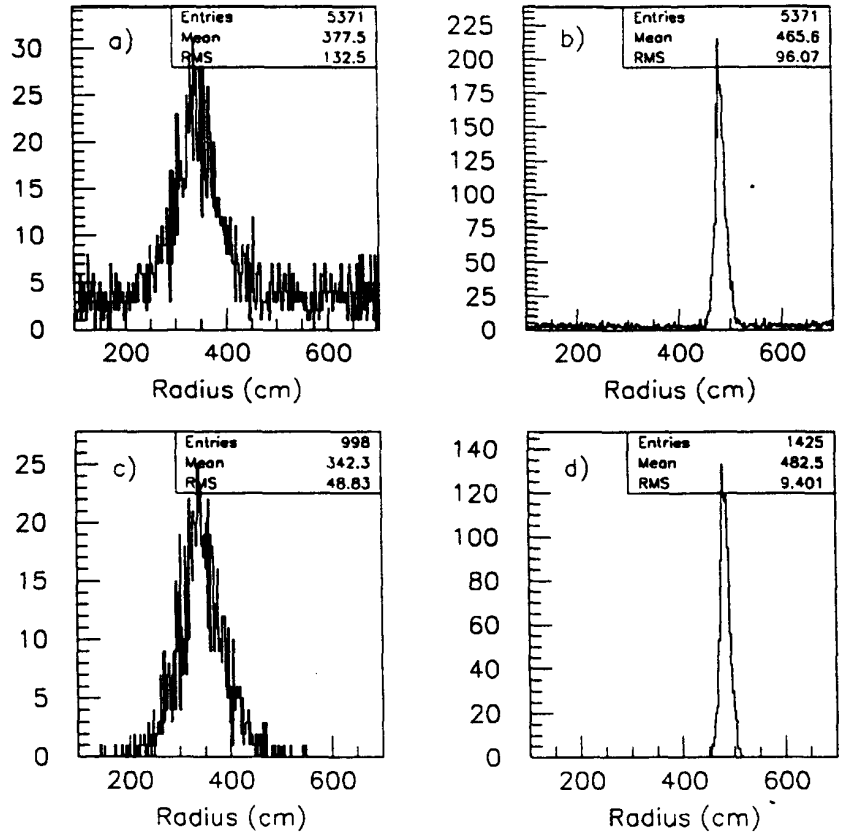

Fig. 4. The r_s distribution of all photons in the event of Fig. 3d combined with track 2 in (a), track 3 in (b); the same after pattern recognition (only unambiguous photons) with track 2 in (c) with track 3 in (d).

$$\cos\theta_p = 2(r/r_s)\sin\alpha - \cos\alpha \qquad (4)$$
$$\tan\phi_p = y_0/x_0$$

A more accurate and general way to reconstruct θ from the hit point (x, y, z) requires that the impact parameter of the particle x_e and the emission point z_e along the track be known [3]. From the tracker data, the interaction vertex (x_v, y_v, z_v) is determined if all secondaries originate at the vertex. The impact parameter of the particle is the obtained from z_v, $\rho_v=\sqrt{(x_v^2+y_v^2)}$ and θ_p as

$$x_e = z_v\sin\theta_p + \rho_v\cos\theta_p \qquad (5)$$

Since the emission point z_e cannot be measured we take it, optimally, to be equidistant between z_v and $z_t=\sqrt{(r^2-x_e^2)}$ i.e

$$z_e=[z_v+\sqrt{(r^2-x_e^2)}]/2 \qquad (6)$$

Using these values of (x_e, z_e) and the measurements of (x, y, z), we calculate the generalized detection angle Ω from the relation

$$\cos\Omega=[(zz_e+xx_e)z_p+(xz_e-zx_e)x_p)]/rr_e \qquad (7)$$

where $r_e=\sqrt{(x_e^2+z_e^2)}$, $z_p=\cos\theta_p$ and $x_p=\sin\theta_p$. From Ω we then find the generalized emission angle Ω_e by solving

$$\Omega=\Omega_\varepsilon+\arcsin(r_e\sin\Omega_e/r)-2\arcsin(r_e\sin\Omega_e/r_m) \qquad (8)$$

using the CERN library routine RZERO to find the zero of a function of one real variable [7]. Knowing Ω and Ω_ε we obtain the Cherenkov emission angles (θ, ϕ) from the relations

$$\begin{aligned}
\cos\theta &= \frac{(zz_p+xx_p)\sin\Omega_e}{r\sin\Omega}-\frac{z_e\sin\Omega'}{r_e\sin\Omega} \\
\sin\theta\cos\varphi &= \frac{(xz_p-zx_p)\sin\Omega_e}{r\sin\Omega}-\frac{x_e\sin\Omega'}{r_e\sin\Omega} \qquad (8) \\
\sin\theta\sin\varphi &= \frac{y\sin\Omega_e}{r\sin\Omega}
\end{aligned}$$

where $\Omega'=\Omega_e-\Omega$. In Fig.s 5a, 5b we show the distribution of two generated Cherenkov angles (tracks 2 and 3 of Fig. 3d) and in Fig.s 5c, 5d the reconstructed angles after pattern recognition. We see from Fig. 5 that the reconstructed distributions are as sharp as the generated distributions (or sharper due to the cuts). The intrinsic width of this distribution will be considered in the next sections.

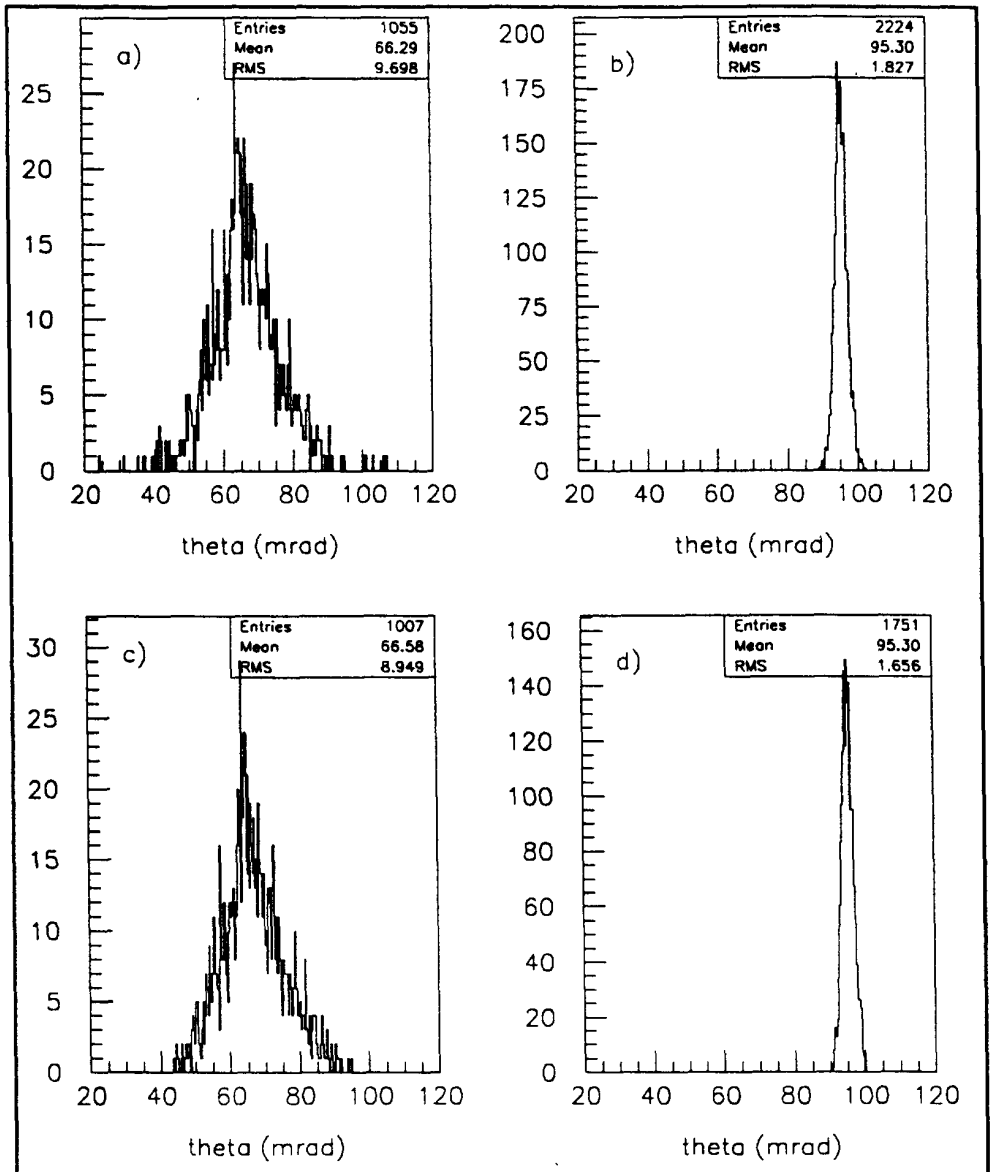

Fig. 5. Distributions of generated Cherenkov angles for tracks 2, 3 of Fig. 3d in (a, b) and the corresponding reconstructed Cherenkov angles in (c, d).

4. MOMENTUM AND MASS DETERMINATION

From the reconstructed Cherenkov angle θ, the velocity β of the particle is found as $\beta=\cos\theta_m/\cos\theta$. Assuming that the mass of a particle has been determined, its momentum is obtained from $p=m\beta\gamma$, where $\gamma=1/\sqrt{(1-\beta^2)}$. Thus, the precision of momentum

determinion relys on the Cherenkov angle precision i.e on the reconstruction accuracy as well as the intrinsic per photon error σ_θ (chromatic, pixel, multiple scattering errors etc.) as detailed below.

Using Eq.'s 5-8 it was found that the reconstructed value of θ agrees with the generated value to an accuracy of 0.01 mrad under the following conditions: chromatic error $\sigma_\theta(E)=0$, emission point error $\sigma_\theta(z_e)=0$, measurement errors $\sigma_\theta(x)=\sigma_\theta(y)=\sigma_\theta(z)=\sigma_\theta(x_e)=0$ the multiple scattering error $\sigma_\theta(ms)=0$. This shows that reconstruction accuracy is sufficient.

The per photon chromatic error, $\sigma_\theta(E)$, may be written as

$$\sigma_\theta(E)=(\partial\theta/\partial n)(dn/dE)\sigma_E \qquad (9)$$

The first factor is the derivative of the Cherenkov relation i.e $\partial\theta/\partial n=1/(n\tan\theta)$. The second factor is the dispersion of the radiator medium and is evaluated from the Lorenz-Lorentz relation [3, 8, 9]. The last factor is the rms width of the detector response ($\sigma_E=\Delta E/\sqrt{12}$ for flat response with bandwidth ΔE). For the proposed detector ΔE=0.8 eV (6.3 to 7.1 eV) with an Argon gas radiator (15 bar, 293K) the chromatic error $\sigma_\theta(E)$ varies between 7 and 0.7 mrad for θ between 10 and 96 mrad, as shown in Fig. 6. For comparison, the corresponding error for a photosensor in the visible region (2 to 2.8 eV) is between 1.6 and 0.2 mrad.

The per photon multiple scattering error $\sigma_\theta(ms)$ depends on the momentum of the particle p, on the length L of the track in the radiator and on the radiation length X_0 of the radiator. It is given as $\sigma_\theta(ms)=(p_{ms}/p)\sqrt{(L/X_0)}$ with p_{ms}=10 MeV [3]. In Fig. 7 we show $\sigma_\theta(ms)$ versus θ for muons, pions, kaons and protons along with the UV chromatic error, for comparison. The calculation used X_0=785 cm for Argon (15 bar, 293K) and (a) a full length track L=50 m or (b) a 10% length track L=5 m. Clearly, the multiple scattering error is dominant for $\theta < 90$ mrad thus, σ_θ will depend on particle type. The width σ_θ can therefore be used for particle identification as shown later in this section.

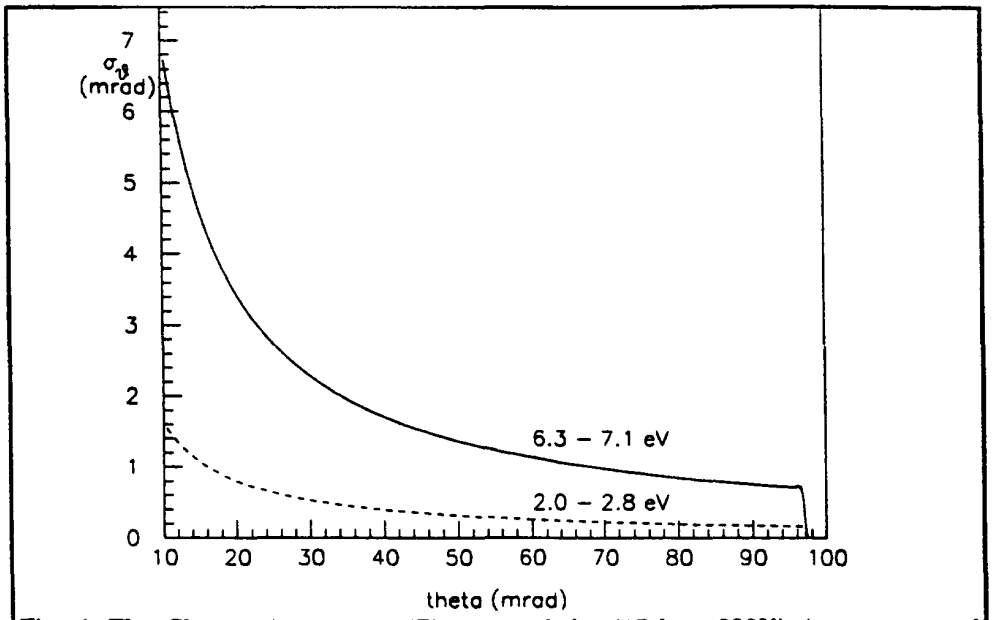

Fig. 6. The Chromatic error $\sigma_\theta(E)$ versus θ for (15 bar, 293K) Argon gas and uniform detector energy acceptance ΔE=0.8 eV for a UV or visible photosensor.

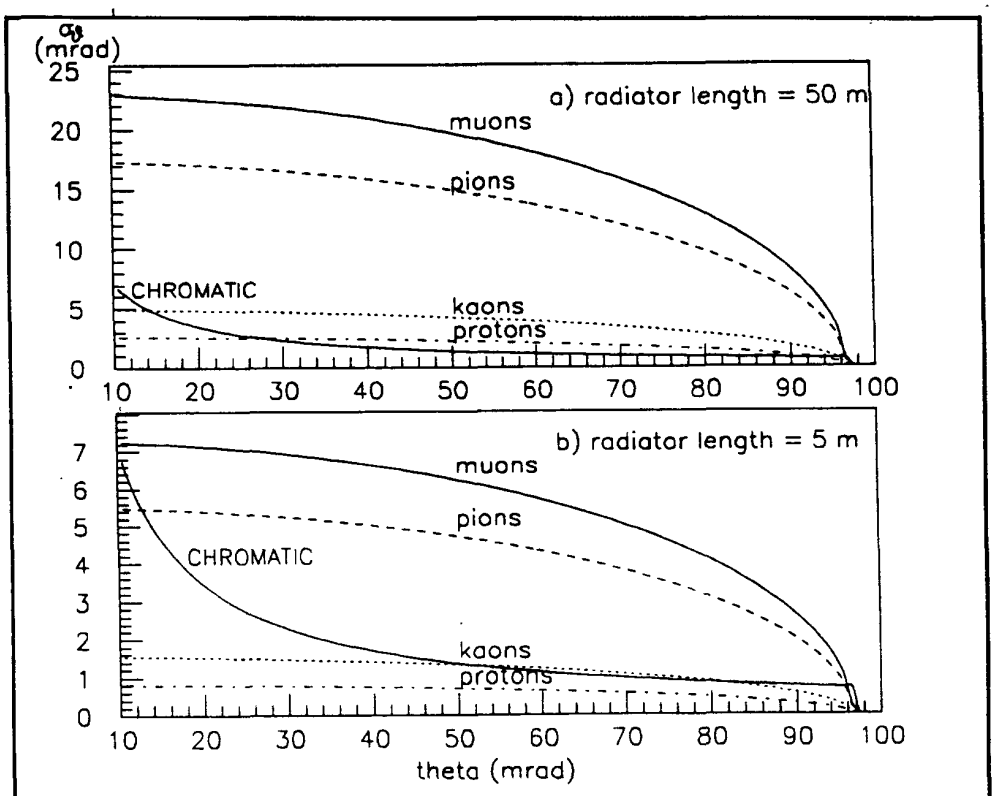

Fig. 7. The multiple scattering error σ_θ vs θ for muons, pions, kaons and protons; the chromatic error is also shown for comparison : a) for L = 50 m ; b) for L = 5 m.

The momentum resolution of a RICH counter is

$$\sigma_p/p=k_r\gamma^2=(\sigma_\theta/\sqrt{N})[\sin\theta\cos\theta/(\sin^2\theta_m-\sin^2\theta)] \qquad (10)$$

with σ_θ the total per photon error, $k_r=n\beta\sigma_\theta/\sqrt{(N_0L)}=\tan\theta\sigma_\theta/\sqrt{N}$, $\gamma=\cos\theta/\sqrt{[\sin^2\theta_m-\sin^2\theta]}$, $p=mc\cos\theta_m/\sqrt{[\sin^2\theta_m-\sin^2\theta]}$, $\cos\theta_m=1/n$ and $\beta=\cos\theta_m/\cos\theta$. The detected photoelectron number is $N=N_0L\sin^2\theta$ where $N_0=(370/eV\text{-}cm)\cdot\varepsilon\Delta E$ is the detector merit factor and $\varepsilon\Delta E=\int QRT dE$ the energy integrated effective quantum efficiency [3]. Note that the resolution depends only on θ, σ_θ and N. For example, a track with $\theta\approx90$ mrad, $N_0\approx89/cm$, L=25 m has $N\approx2000$ and, for $\sigma_\theta\approx2$ mrad, $k_r=\sigma_\beta/\beta\approx4.1\cdot10^{-6}$. Its momentum would then be determined with error $\sigma_p/p=0.26\%$, an excellent result if it can be attained. The momentum of such a particle is p=29.8(m) GeV/c.

In the normal use of RICH counters the particle track length L in the radiator is near constant. The situation here is quite different since L can vary from (0-50) m depending on the point where the neutrino interacts hence N depends on L as well as on β and so the RICH constant k_r will be variable. However, in case of multiple scattering dominance (MSD) we use in Eq. 10 the angular error $\sigma_\theta=\sigma_\theta(ms)=(p_{ms}/p)\sqrt{(L/X_0)}$ with $p_{ms}=.01$ GeV and obtain for the invariant momentum resolution

$$\begin{aligned} m(\sigma_p/p)&=[p_{ms}/\sqrt{(N_0X_0)}]n\gamma \qquad (11)\\ &=[p_{ms}/\sqrt{(N_0X_0)}](\cos\theta/\cos\theta_m)/\sqrt{[\sin^2\theta_m-\sin^2\theta]} \end{aligned}$$

and solving for the mass

$$\begin{aligned} m&=p_{ms}\sqrt{(L/X_0)}/\sigma_\theta\beta\gamma \qquad (12)\\ &=(p_{ms}/\sigma_\theta)\sqrt{(L/X_0)}\sqrt{[\sin^2\theta_m-\sin^2\theta]} \end{aligned}$$

Notice that the L dependance of the invariant resolution function $m(\sigma_p/p)$ cancels because k_r is inversely proportional to $\sqrt{L}$ while multiple scattering is proportional to $\sqrt{L}$. Note also that $m(\sigma_p/p)$

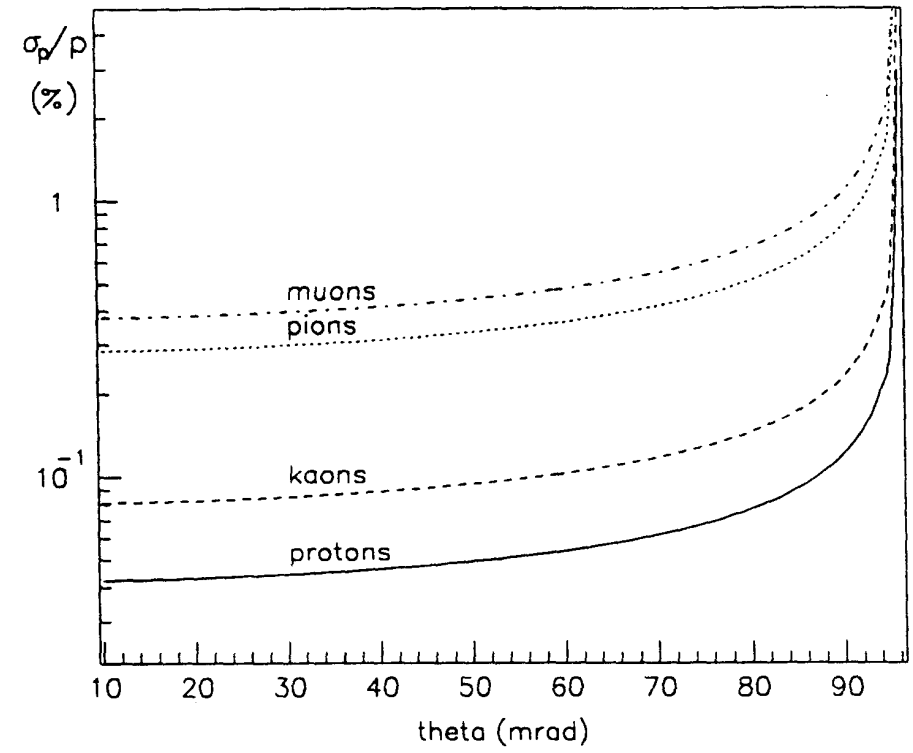

Fig. 8. The momentum resolution σ_p/p versus the Cherenkov angle θ for muons, pions, kaons and protons assuming only multiple scattering errors (Eq. 11).

depends linearly on γ, like the p dependance of (σ_p/p) of a magnet. For the counter considered here the constant term of Eq. 11, $p_{ms}/\sqrt{(N_0X_0)}=3.8\cdot10^{-5}$ GeV, thus the invariant resolution $m(\sigma_p/p)$ varies from $(4.0\text{-}11.4)10^{-4}$ Gev for θ between (10-90) mrad. The momentum resolution σ_p/p is plotted in Fig. 8 for muons, pions, kaons and protons. We note that (σ_p/p) is everywhere excellent ($\leq$ 1%) reaching 1.08% for muons with θ=90 mrad. The momenta corresponding to θ=90 mrad are p_μ=3.14, p_π=4.18, p_K=14.73 and p_p=28.04 GeV/c. For kaons and protons MSD doesnt apply above 90 mrad but these momenta are already quite high for the intended neutrino beams. For muons and pions MSD extends up to about θ=95 mrad (see Fig. 7) corresponding to momenta p_μ=7.59, p_π=10.1 GeV/c with the still good momentum resolution of 2.61%

and 1.96%, respectively. This range of momenta would be quite appropriate for incident neutrino beams in the 10-30 GeV/c range.

We consider all Cherenkov images from 209 above threshold reconstructable tracks (70 muons, 135 pions, 4 kaons) from a mixture of 144 CC $\nu_\mu X$ and $\nu_\tau X$ interactions in Argon gas (15 bar, 293K) for E_ν between 13.5 to 40 GeV/c. The images were generated with chromatic errors $\sigma_\theta(E)=\Delta E/\sqrt{12}$ and the detector pixel errors $\sigma_\theta(x)$, $\sigma_\theta(y)$, $\sigma_\theta(z)$. The impact parameter $\sigma_\theta(x_c)$ and emission point $\sigma_\theta(z_e)$ errors were not included because they are calculable and their contribution will be small. The chromatic bandwidth was ΔE=0.8 eV (6.3 to 7.1 eV), the pixel sizes $\Delta x=\Delta y$=30 mm and Δz=0.1 mm. The beam was constrained to interact at the middle of the radiator (z_v=25 m) but, the transverse interaction point was chosen randomly. The use of a constant pathlength L=25 m should not bias the result since Eq.s 11, 12 are L independant. The emission point error $\sigma_\theta(z_c)$ is also ignored here but we know its contribution is much less than chromatic. In Fig. 9 we plot seperately the momentum resolution σ_p/p from Eq. 10 for (a) muons, (b) pions and (c) kaons vs the reconstructed Cherenkov angle θ. This assumes that the particle mass is known (see below). The resolutions agree very well with the curves from Eq. 11 (see Fig. 8) thus showing that MSD is applicable. We stress that each track has been pattern recognized and reconstructed by the methods given above thus give a good estimate of what can be experimentally attained. We see that almost over the full range of Cherenkov angles (30-95 mrad) the momentum resolution is excellent (< 4%).

To determine the mass spectrum we use the reconstructed values of σ_θ, L and θ in Eq. 12 (applicable if MSD is true). The mass spectrum for the above 209 track sample is shown in Fig. 10. We see the kaons are identified and even pions and muons are resolved but, some overlap remains. Recall however, from Fig. 1, that an external muon identifier will be able to positively identify the muons thus, all charged particles should be identified. Protons are not seen because of their high threshold (p=9.73 GeV/c).

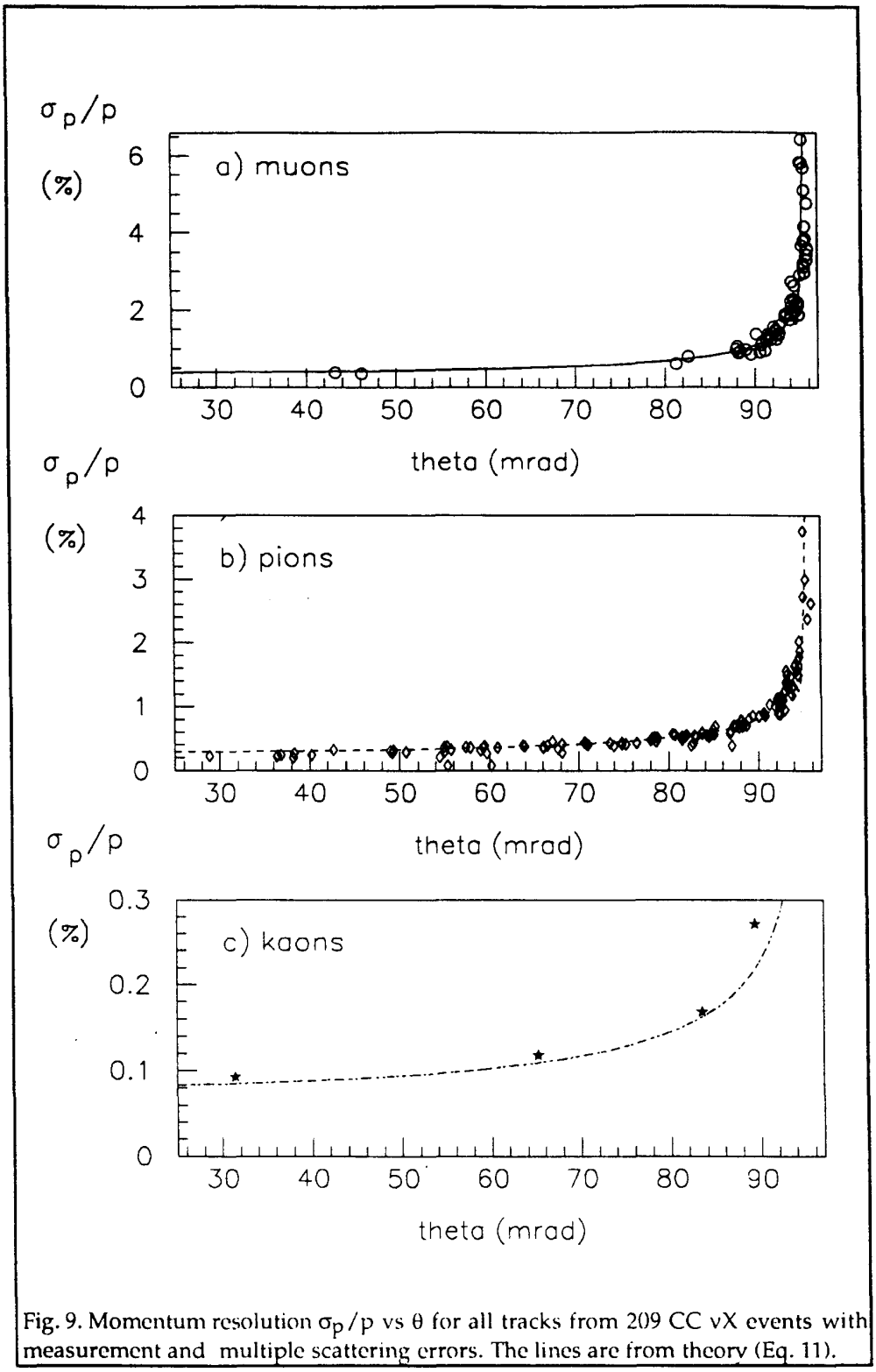

Fig. 9. Momentum resolution σ_p/p vs θ for all tracks from 209 CC νX events with measurement and multiple scattering errors. The lines are from theory (Eq. 11).

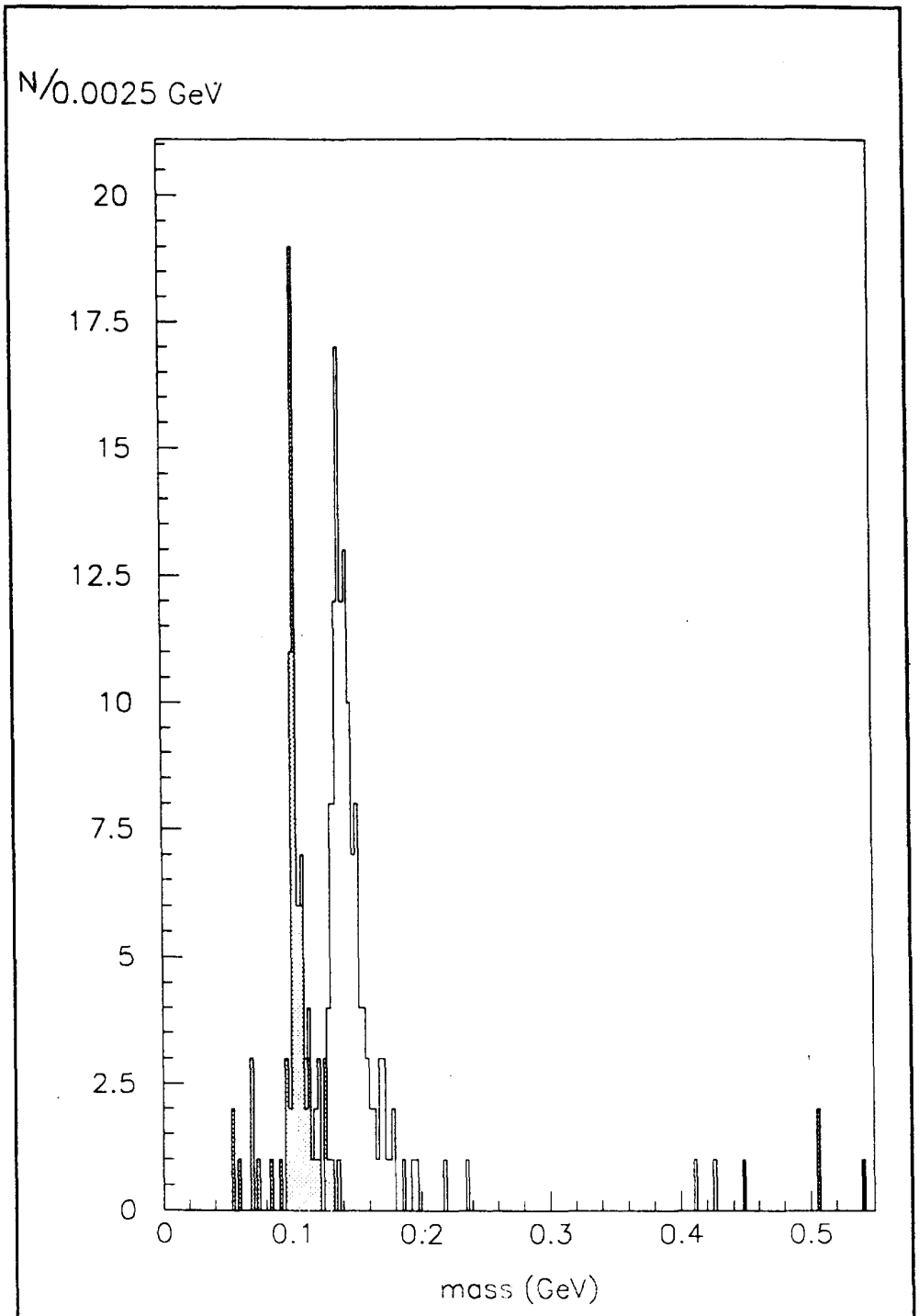

Fig. 10. The mass spectrum for the tracks (Fig. 9). The mass was calculated via Eq. 11 from σ_θ, L and the reconstructed θ.The muon (kaon) tracks are shaded (black).

5. ν_τ SIGNALS AND ν_μ BACKGROUND

A simulation of 500 CC $\nu_\mu p \text{---} \mu X$ events using PYTHIA 5.701 gave the (p, p_t) scatter plot shown in Fig. 11. Here we only require that the muon be above threshold i.e $p_\mu > 1$ GeV/c. In Fig. 12 we show 500 CC $\nu_\tau p \rightarrow \tau X$, $\tau \rightarrow \mu X'$ events again requiring $p_\mu > 1$GeV/c (420/500 muons pass this cut). We see a large region of low p_t events which are not present in the direct process. If we impose a cut of $p_t < 0.9$ GeV/c (the horizontal lines in Fig.s 11, 12) then 4 direct muons survive (0.8%) compared to 284 indirect muons (56.8%). However all the direct muon survivors have $p < 2$ GeV/c hence, by cutting above 2 GeV/c (the vertical lines in Fig.s 11, 12) no direct muons (0%) but 190 indirect muons survive (38%). Thus, this device can strongly discriminate against ν_μ events (0/500) with still good efficiency (190/500) for ν_τ events.

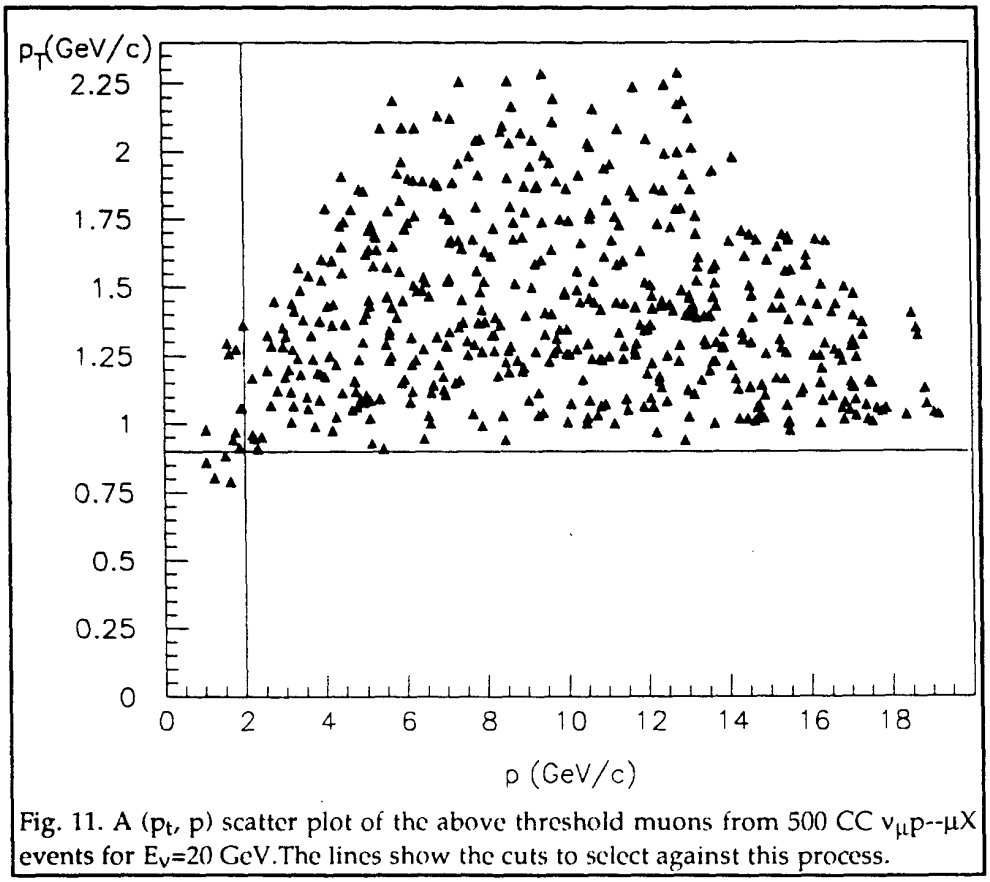

Fig. 11. A (p_t, p) scatter plot of the above threshold muons from 500 CC $\nu_\mu p \text{--} \mu X$ events for E_ν=20 GeV.The lines show the cuts to select against this process.

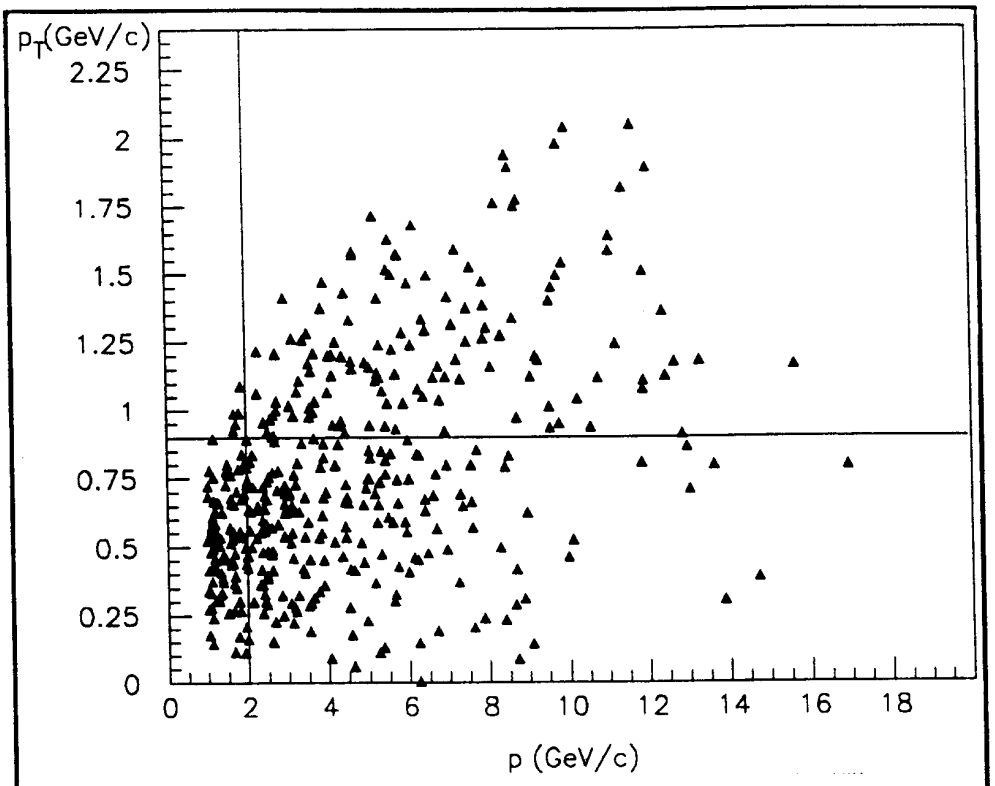

Fig. 12. A (p_t, p) scatter plot of above threshold muons from 500 CC $\nu_\tau p \rightarrow \tau X$, $\tau \rightarrow \mu X'$ events for E_ν=20 GeV. Below and right of the dotted lines has no direct muons.

6. RATES

The rates are based on a recent simulation of long baseline neutrino beams for Gran Sasso and NESTOR [10] using a 160 GeV/c proton beam on Be rod targets target followed by a 20 GeV/c coaxial "horn" collector. It predicts at Gran Sasso a Gaussian ν_μ beam with radial width σ_r=3 km, average neutrino energy $\langle E_\nu \rangle$=15 GeV and width $\sigma_{E\nu}$=5 GeV. The ν_e, ν_μ, ν_e contamination of this beam was 0.9%, 3.5%, 0.3% respectively. Even though this contamination is not a background for our technique, we nonetheless assume that the minimum detectable mixing is ≈1% thus requiring at least 100 potential events.

The flux is such that 200 events/kton may be expected for $3 \cdot 10^{19}$ protons on target per year. An array of nine RICH counters (q.v. Fig. 1) would contain 3.6 ktons of target mass hence produce

720 ν_μ or 49 ν_τ events/y (full mixing, 38% tagging efficiency, 18% branching ratio $\tau \rightarrow \mu$). This would probe $\Delta m^2 = m_{\nu\tau}^2 - m_{\nu\mu}^2$ down to $2.3 \cdot 10^{-3}$ eV^2 and the mixing parameter $\sin^2(2\theta)$ down to 0.28.

If, as seems likely, the $\tau \rightarrow [\pi + (n\pi^0) + \nu_\tau]$ mode can be used (50% branching ratio) the event rate increases to 186/y, Δm^2 decreases to $1.2 \cdot 10^{-3}$ eV^2 and $\sin^2(2\theta)$ to 0.15.

It is unlikely that the $\tau \rightarrow e\nu_e\nu_\tau$ mode (18% branching ratio) can be used notwithstanding the low background ($\approx$1% from ν_e or $\bar{\nu}_e$) because direction, but not momentum, of an electron can be determined in RICH (since $\beta \approx 1$). The electron may be tagged by $\theta \approx \theta_{max}$ and a large image width σ_θ moreover, it may start to shower in the Argon gas (X_0=7.85 m).

A gamma may be tagged because its conversion vertex will be quite seperate from the hadron vertex and its image (due to the e^+e^-) will have twice the hit density per unit path length.

The large 9 tank array (60 x 60 x 50 m^3) can be sited at the external laboratory area of the Gran Sasso complex.

7. THE DETECTOR

The experimental problem is large but straightforward. Stainless steel tanks (20 m diameter, 50 m length) to contain the (15 bar, 293 K) Argon gas are constructable.

The requisite mirrors with 100 m radius of curvature can be produced in 1 m^2 sections (314 per tank) and aluminized with MgF_2 overcoating for good UV reflectivity.

The large surface area tracker can be made of resistive plate chambers because of their good spatial resolution (σ_x=0.25 mm) and fast response (σ_t=2 ns). Since these cheap, large areas devices are the subject of considerable R&D effort for LHC, their results could be directly applicable here [11]. The absorber should be 0.8 m thick iron corresponding to the range of a 1 GeV/c muon. This represents λ=4.7 interaction lengths or about 1% contamination of hadrons this, in addition, to the particle separation obtained from the RICH counter (see Fig. 10).

The transparency of Ar gas in the (6.3-7.1) eV region should be good but measurements over 50 m distance (with Ar gas of density .025 g/cm^3) are not available. We have however measured the transparency of liquid Krypton (density ρ=2.6 g/cm^3) and found l_{abs}=3 m at E=6.7 eV [12]. The density of (15 bar, 293 K) Kr gas is 0.05 g/cm^3 or 52 times less dense than Kr liquid hence, l_{abs}=156 m for (15 bar, 293 K) Kr gas. Since the Argon resonance absorption energies are higher than those for Krypton, we can confidently infer $l_{ab} \approx$200 m for Ar gas (15 bar, 293 K). This implies a UV light transmission T≈70% for the average photon pathlength of 75 m, sufficient for this experiment.

Clearly, the essential elements for this detector are the $3 \cdot 10^5$ photosensors (per tank). Photomultipliers (PMs) would suffice nicely (even giving visible light response) but at a price of ≈500 SF (for a 25 mm ϕ PM) they would be much too expensive (150 MSF/tank, 1.35 GSF/9 tanks).

Another solution could be the Fast RICH detectors with CsI reflective photocathodes (PCs) and gas amplification, now being developed for B-Factories [4]. The full photodetector system with VLSI electronics is expected to cost 8 SF/ channel thus 2.4 MSF/tank. The cost is supportable for one B-Factory detector but for nine tanks would be still on the high side (22 MSF/9 tanks).

The new development of Hybrid Photo-Diodes (HPDs) [13] looks quite promising if coupled home-made CsI transmittive photocathodes [14] vacuum evaporated on UV transparent fused quartz windows. Since these PCs can be exposed to air their fabrication does not require the high technology and expense associated with visible light PMs. Since HPDs operate in vacuum, the CsI PCs can be cleaned by pumping and getters installed. Gain is obtained by accelerating the photoelectrons to ≈13 kV with impact onto a Silicon wafer target leading to a charge output of $3 \cdot 10^3$ e. Fabrication of a 64 element HPD with a 200 x 200 mm quartz window (pixels of 25 x 25 mm^2) and a CsI transmittive PC with 64 separate Silicon wafer targets (2 x 2 mm^2 at 0.1 SF/mm^2) is

under study. Readout could be obtained with already developed Silicon strip electronics such as the Amplex chip (128 channels for ≈200 SF). This chip is free running and can be used without an external start signal. With some R&D effort it is thought that the price can be brought down to ≈1 SF per channel hence about 3 MSF for the 9 tank (3.6 kton) device. At this level, the mechanical, tracking and optical elements dominate the total price.

8. CONCLUSIONS

We believe we have demonstrated that large RICH counters can measure neutrino interactions by imaging the above threshold ($\gamma > 10$) secondary particles. These images determine particle direction and momentum (i.e. p and p_t) and mass but not the sign of the charge. Selection of $\tau \rightarrow \mu$ (or π) decays is possible by cuts in the (p, p_t) plane.

REFERENCES

[1] S. Parke, "Overview of accelerator long baseline neutrino oscillation experiments" in the Moriond Workshop on Neutrino Physics Proceedings, 30/1-6/2/93 at Villars, Switzerland.

[2] A. Zichichi, "Perspectives of Underground Physics: The Gran Sasso Project", CERN-EP/88-28.

[3] T. Ypsilantis and J. Séguinot, "Theory of Ring Imaging Cherenkov Counters", Nucl. Instr. and Meth. A343 (1994) 30.

[4] R. Arnold, Y. Giomataris, j.L. Guyonnet, A. Racz, J. Seguinot and T. Ypsilantis, Nucl. Instr. and Meth. A314 (1992) 465.

[5] F. Bloch, "Monte Carlo simulation $\nu_\tau p$ and $\nu_\mu p$", CERN LAA/MSL-93-05.

[6] CHORUS Collaboration, M. de Jong et al., "A New Search for $\nu_\mu \rightarrow \nu_\tau$ Oscillations", CERN-PPE/93-131.

[7] CERN Computer Program Library 6.16, (30/5/1989)

[8] T. Ypsilantis, "Particle Identification at Hadron Colliders", CERN-EP/89-150, Symposium on Particle Identification at High Luminosity Hadron Colliders, Fermilab, 5-7 April 1989.

[9] J. Séguinot, "Les compteurs Cherenkov: Applications et limites pour l'identification des particules. Développements et perspectives", CERN-EP/89-92 and College de France LCP/89-25.

[10] S. Anassontzis et. al, Proceedings of the 3rd NESTOR International Conference, 19-21 October, 1993, Pylos, Greece. Athens University Press.

[11] J. Crotty, J. Lamas Valverde, G. Laurenti, M.C. S. Williams and A. Zichichi, " Further studies of avalanche mode operation of resistive parallel plate chambers", CERN PPE/94-39, CERN/LAA-MC 94-12, in press Nucl. Instr. and Meth.

[12] J. Seguinot, J. Tischhauser and T. Ypsilantis, "Measurements of the transmission of liquid Xenon and Krypton versus photon wavelength". In preparation.

[13] R. De Salvo CLNS 87-92, Cornell University, Ithaca, NY. See also R. De Salvo et. al., Nucl. Instr. and Meth. A315 (1992) 375.

[14] C. Lu and K. T. McDonald, Nucl. Instr. and Meth. A343 (1994) 135.

Un RICH de grande surface pour l'oscillation de neutrinos sur une grande distance

Résumé

Un grand compteur RICH put servir à la fois de cible et de détecteur pour une expérience d'oscillations de neutrinos sur une grande distance. Un radiateur cylindrique de 20 m de diamètre et de 50 m de long rempli d'argon gazeux à 15 bar et 293° K possède un seuil Cerenkov $\gamma_{\rm th} = 10$ et contient 400 tonnes de cible sensible aux interactions de neutrinos. Une particule traversant avec $\beta \approx 1$ produira 4000 photoélectrons sur une image annulaire, ce qui déterminera son moment à 4 % près à 20 GeV (en supposant la particule identifiée). L'image RICH détermine aussi la direction de la particule, c'est à dire son p_T aussi bien que son p, si bien que les muons directs (issus de ν_μ) et les indirects (issus de ν_τ peuvent être séparés par des coupures dans le plan (p, p_T).

Une simulation Monte-Carlo des images RICH a été faite en utilisant un nouvel algorithme dans GEANT pour engendrer des photons Cerenkov. Une méthode de reconnaissance de formes basée sur la projection stéréographique est présentée. La vitesse de la particule est déterminée à partir de l'angle Cerenkov, alors qu'en même temps l'identification est identifiée par la largeur de la distribution de l'angle Cerenkov. Cette largeur dépend de la masse pour des particules de même vitesse parce que l'erreur sur l'angle Cerenkov est dominée par la diffusion multiple, si bien que le compteur RICH peut déterminer le type de particule ainsi que son moment.